JACS
JOURNAL OF THE AMERICAN CHEMICAL SOCIETY
Article
pubs.acs.org/JACS

Drug Uptake Pathways of Multidrug Transporter AcrB Studied by Molecular Simulations and Site-Directed Mutagenesis Experiments

Xin-Qiu Yao,[†] Nobuhiro Kimura,[‡] Satoshi Murakami,[‡] and Shoji Takada*[,†,§,∥]

[†]Department of Biophysics, Graduate School of Science, Kyoto University, Kyoto 606-8502, Japan
[‡]School and Graduate School of Bioscience and Biotechnology, Tokyo Institute of Technology, Yokohama 226-8501, Japan
[§]CREST, Japan Science and Technology Agency, Kawaguchi, Saitama 332-0012, Japan
[∥]Advanced Center for Computing and Communication, RIKEN, Wako Saitama 351-0198, Japan

Supporting Information

ABSTRACT: Multidrug resistance has been a critical issue in current chemotherapy. In *Escherichia coli*, a major efflux pump responsible for the multidrug resistance contains a transporter AcrB. Crystallographic studies and mutational assays of AcrB provided much of structural and overall functional insights, which led to the functionally rotating mechanism. However, the drug uptake pathways are somewhat controversial because at least two possible pathways, the vestibule and the cleft paths, were suggested. Here, combining molecular simulations and site-directed mutagenesis experiments, we addressed the uptake mechanism finding that the drug uptake pathways can be significantly different depending on the properties of drugs. First, in the computational free energy analysis of drug movements along AcrB tunnels, we found a ligand-dependent drug uptake mechanism. With the same molecular sizes, drugs that are both strongly hydrophobic and lipophilic were preferentially taken in via the vestibule path, while other drugs favored the cleft path. Second, direct simulations realized totally about 3500 events of drug uptake by AcrB for a broad range of drug property. These simulations confirmed the ligand-dependent drug uptake and further suggested that a smaller drug favors the vestibule path, while a larger one is taken in via the cleft path. Moreover, the direct simulations identified an alternative uptake path which is not visible in the crystal structure. Third, site-directed mutagenesis of AcrB in *E. coli* verified that mutations of residues located along the newly identified path significantly reduced the efflux efficiency, supporting its relevance in *in vivo* function.

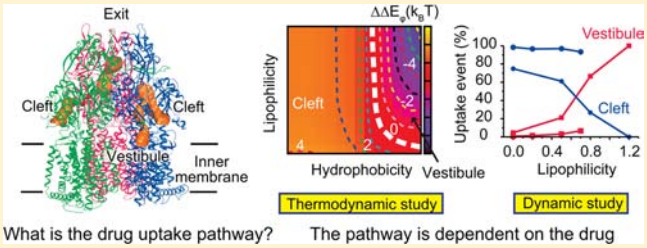

INTRODUCTION

Multidrug resistance of pathogenic bacteria mediated by various transporting systems has attracted increasing attention in recent years.[1−3] In *Escherichia coli*, a major efflux pump responsible for both intrinsic and elevated levels of drug resistance contains three components: the inner-membrane transporter AcrB, the outer-membrane channel TolC, and the lipoprotein AcrA which acts as an adaptor coordinating the motions of AcrB and TolC.[4−8] *In vivo*, the three components associate together forming a stable tripartite complex spanning the periplasm.[9−13] In the complex, AcrB plays the central role; it recognizes and actively exports various noxious compounds including a broad range of antibiotics toward medium, using the proton motive force.[14,15] AcrB is also one of the best-characterized transporters in both experiment and computation and is a prospective target of future drug design.

X-ray crystallography provided much of atomic structural insights on AcrB.[16−19] AcrB forms a homotrimer and each monomer is divided into three domains (Figure 1A). The cytoplasmic-side transmembrane helix (TM) domain localizes the protein in the inner membrane and is responsible for the proton transfer across the membrane. The periplasmic-side head called TolC-docking domain is supposed to bind TolC participating to a central channel, and the middle periplasmic porter domain takes the major responsibility for drug binding. Large internal cavities containing possibly multiple binding sites in the porter domain explain the diversity of AcrB substrates.[17,20,21]

Surprisingly enough, the crystal structures of AcrB homotrimer solved in 2006−2007 display asymmetric conformations, which suggested the functionally rotating mechanism.[17−19] One monomer has an open pocket (called the distal binding pocket) and thus can bind drugs, such as minocycline, at the porter domain (designated as the binding state or the B state). In another monomer, the pocket is shrunk, but there is a clear tunnel from the pocket to the TolC docking domain which suggests the state for drug extrusion (designated as the extrusion state or the E state). The last monomer takes a conformation similar to the B state except that the distal binding pocket is closed, which thus may wait for the drug access (designated as the access state or the A state). The entire trimer thus represents the "ABE" state, where each letter indicates the state of one protomer. In the context of the alternating-access model,[25] the A

Received: October 25, 2012
Published: April 29, 2013

   dx.doi.org/10.1021/ja310548h | J. Am. Chem. Soc. 2013, 135, 7474−7485

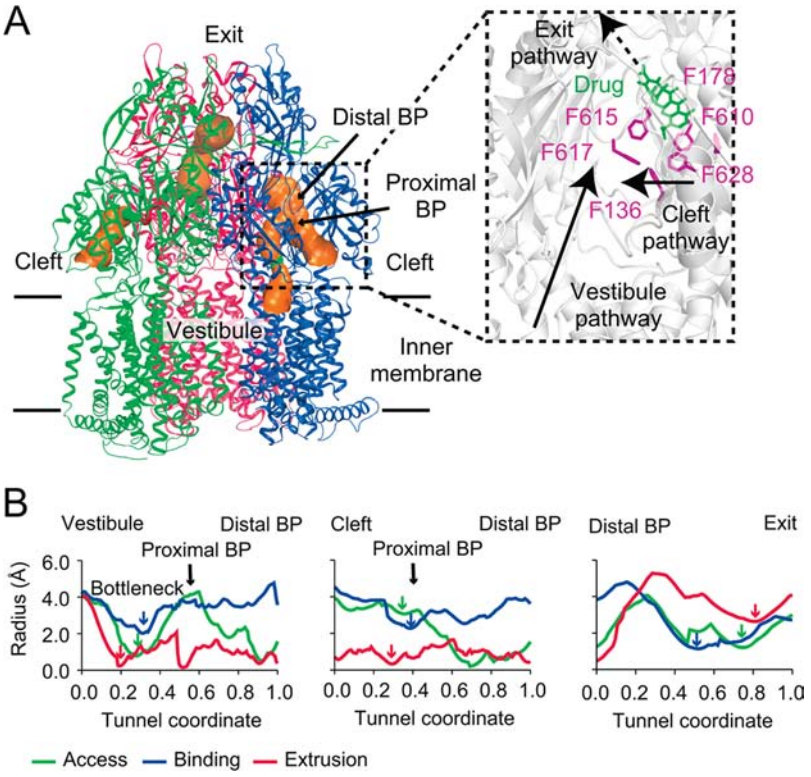

Figure 1. Tunnels in AcrB. (A) The internal surface of identified tunnels in AcrB homotrimer calculated by HOLE[22] with colors indicating the radius of cavity. Red and green regions of the surface are much narrower than the orange region. The enlarged distal binding pocket (BP) displays a minocycline (green) associated with the six key phenylalanines (magenta). AcrB molecules in green, blue, and red, are the A, B, and E states, respectively. The graph of the overall AcrB with characterized tunnels was generated by VMD,[23] and the enlarged BP by PyMol.[24] (B) The radius of cavity along each tunnel measured by HOLE for the vestibule (left), cleft (middle), and exit (right) tunnels. The tunnel coordinate is defined by the direction connecting the two ends of the tunnel.

and B states are essentially the inward-facing conformation, while the E state corresponds to the outward-facing state. The described asymmetric AcrB homotrimer complex suggested a particular mode of functions, called the functionally rotating mechanism: If each protomer changes its state in a cyclic way A→B→E→A, the protomer may export one drug molecule out of the cell upon the state change to the E state. As a trimer, it may change the conformations concertedly, for example, from the ABE to the BEA forms, resulting in a 120° rotation in the functional space. The functionally rotating mechanism is quite plausible, and its feasibility was confirmed by both *in vivo* experiment[26−28] and molecular simulations.[29,30]

More recently, structures for AcrB cocrystallized with various drugs provided further clues on the multisite drug binding and drug pathways within AcrB.[31,32] Some drugs were found to bind in a newly identified proximal binding pocket, located closer to the membrane and separated from the distal binding pocket by a loop. The translocation of drugs from the proximal to the distal binding pockets may be catalyzed by the conformational transition from the state A to B. Such a stepwise binding process has also been predicted by a theoretical study.[33]

Despite much of structural insights, the drug uptake pathways in AcrB are poorly understood and controversial. Because lipophilic antibiotics tend to stay on the membrane surface, it was anticipated that the drug uptake of AcrB was mainly from the boundary between the porter domain and the outer leaflet of the inner membrane.[15−17] Then, a groove formed between TM8 and TM9 near the "vestibule" was identified, from where the crystal structures show a narrow tunnel going to the proximal and the distal binding pockets. This tunnel is denoted by "vestibule pathway" here. The proximal binding pocket may represent an initial stage of the drug uptake. On the other hand, AcrB-drug cocrystals in a form of three-fold symmetry,[34,35] as well as site-directed mutagenesis studies,[34] suggested an alternative drug uptake pathway via the external cleft, called "cleft pathway", which exists between the PC1 and PC2 subdomains. This route connecting the cleft with the distal binding pocket is shorter and wider, compared to the vestibule pathway. But, the cleft is in periplasm and away from the membrane indicating that drugs need to spontaneously dissociate from the membrane to use this path. Notably, recent covalent-labeling experiment supported both vestibule and cleft pathways, implying a multiple-pathway mechanism of drug uptake in AcrB.[36,37]

The purpose of this study is to elucidate the drug uptake pathways by molecular dynamics (MD) simulations together with site-directed mutagenesis experiments. Although several MD simulations have been performed, none of them addressed the problem of drug uptake directly.[29,38−46] Previously, we have studied the functional rotation and drug export in AcrB using coarse-grained (CG) molecular simulations.[30] With a similar, but more accurate, model, we performed comprehensive study of drug uptake using both free energy analysis and dynamic simulations. Unexpectedly, we found a novel uptake and binding pathway by dynamic simulations. The pathway was then assessed by site-directed mutagenesis experiments.

dx.doi.org/10.1021/ja310548h | J. Am. Chem. Soc. 2013, 135, 7474−7485

RESULTS

Tunnels in AcrB. Structural analysis of AcrB homotrimer discovered multiple internal tunnels, which are potential pathways for drug transport.[21,31,32,36,37,47] Here, we focused on three types of tunnels connecting the distal binding pocket with either inside or outside of the cell (Figure 1A): The vestibule tunnel has one end opened at the TM8/TM9 groove proximal to the outer leaflet of the inner membrane. The cleft tunnel has its end opened near the cleft, well above (~15 Å) the membrane. These two tunnels merge from the proximal to the distal binding pocket. The exit tunnel goes from the distal binding pocket to the exit and the central channel formed by AcrB and TolC. Among many crystal structures, widths of tunnels are somewhat different, and in this study we chose the one (PDB code 2J8S)[19] which has the most clearly open vestibule tunnel.

The breadth of each tunnel significantly varies among the three states (Figure 1B). The vestibule tunnel, for example, is evidently open in the B state with the radius of cavity at tunnel bottleneck ~2 Å. It is, however, almost completely closed in the E state. The A state has the open entrance near the vestibule and the proximal binding pocket, but a bottleneck between the two is very narrow (<1 Å). On top, it has substantially shrunk distal binding pocket. Similar trend was observed for the cleft tunnel except that the bottleneck here is not tight in the A state (~3 Å). Interestingly, the cavity of the proximal binding pocket in the A state is slightly larger than that in the B state, probably explaining the exclusive binding of large substrates in the proximal binding pocket in the A state.[31,32] Finally, the exit tunnel is open only in the E state, with the bottleneck radius of ~2.6 Å.

While the exit tunnel is obviously responsible for drug export, which tunnel, vestibule, or cleft is used for drug uptake? In addition, is there another pathway that is closed in the crystal structure but could be available due to the fluctuation or ligand-induced allostery? To address these questions, we studied both the free energy surface and the dynamics of drug uptake in AcrB by molecular simulations.

Computational Modeling. Current computational studies of AcrB-catalyzed drug transport fall into three categories: all-atom MD simulations,[29,38,40,41,44−46] molecular docking/mapping,[21,33] and CG molecular simulations.[30,39] Compared to the former two types of methods, which were usually based on an atomistic description of the system, the CG method is distinguished by its high computational efficiency. CG MD simulations can reproduce large-scale molecular motions orders-of-magnitude longer time scale than that all-atomic MD can reach. In a previous work, employing a structure-based CG model, we could investigate the functional rotation and drug export in AcrB that are long-time scale events.[30] In this model, each amino acid residue was represented by one bead placed on the C_α. The interaction between beads was developed based on the energy landscape perspective of the protein[48] and took the relevant crystallographic structure of AcrB as the reference point of minimal potential energy. The success of the model in reproducing the functional rotation and subsequent drug export suggests that it could be also useful in studying the problem of drug uptake.

In present work, the CG protein model introduced previously has been improved in two aspects. First, each amino acid (except for glycine) is represented by two beads: Besides the C_α bead, a second bead is introduced at the center of mass of the side chain. The new model accounting for higher resolution of amino acid gives a better description of the geometry of protein surface and therefore is more accurate in simulating the diffusion of drug molecules inside the protein. Second, a systematic parametrization is adopted instead of using empirical model parameters. The method, called atomic-interaction based coarse-grained (AICG) model,[49] concisely realizes the globally funnel-shaped energy landscape for any given reference structure and simultaneously approximates atomistic interactions and fluctuations via a multiscale algorithm.[50]

In this work, we used three drugs molecules in the computation: minocycline, acriflavine, and novobiocin, which are all typical substrates of AcrB but have different molecular sizes and hydrophobicity. We adopted a similar CG model as used in previous work for minocycline[30] and developed new models for acriflavine and novobiocin. Specifically, we chose the carbon atoms that best characterize the shape of the molecule as CG beads and then connected the beads by virtual bonds. All drugs were modeled as rigid linear molecules. The number of beads for each drug was determined based on a consistent level of coarse-graining, i.e., about one bead per six heavy atoms. A similar hydrophobic energy term introduced before[30] was also employed to account for the attractive interaction between protein and drug. The drug here, however, had additional attractive interaction with an implicit membrane modeled by a simple rounded square well potential. The strengths of the drug−protein and the drug−membrane interactions were characterized with two independent parameters, c_P and c_M, respectively. With respect to real drugs, c_P corresponds to the theoretical partition coefficient between simple organic solvent and water, called clogP and denoted here by "hydrophobicity", while c_M is related to the partition of the drug into the realistic membrane bilayer ("lipophilicity"). Although the two terms have been interchangeably used, there are increasing evidence showing that they are not always the same.[51] Given that AcrB has broad range of substrates, instead of deciding a single set of c_P and c_M values that best approximate one drug, we scanned these two parameters for a broad range. By this, we can obtain more comprehensive insights on multidrug recognition of AcrB.

More technical details are found in the Experimental section and SI text.

Free Energy Analysis and the Ligand-Dependent Uptake Mechanism. Using the CG model, we first performed free energy analysis along each of the three tunnels that are connected to the distal binding pocket of AcrB. For each of the three tunnels, we defined a simple reaction coordinate (RC) and calculated free energy profiles for the drug to move along the RC. For the vestibule and exit tunnels, the RCs are the distances along single lines approximately parallel to the tunnels. For the cleft pathway, the RC is divided into two parts. First, starting from the membrane-embedded position out of AcrB, the drug is moved to the periplasm along the direction normal to the membrane surface. Second, in parallel to the membrane surface, the drug is moved into the distal binding pocket of AcrB via the cleft gate (Figure S1). For each of the pathways, we performed the standard umbrella sampling with one set of c_P and c_M, while the free energy results in the range of $0.0 \le c_P \le 1.4$ and $0.0 \le c_M \le 1.4$ were obtained by the standard reweighting method.[52] The investigation here focused on the effects of c_P and c_M, and so the drug size was fixed to that of minocycline. The resulting free energy profiles are shown in Figures 2A, S2, and S3. All the free energy profiles were adjusted to have the same reference point, making it possible to compare any two points along the RCs.

In the B state, either along the vestibule or the cleft pathway, there exist two major free energy minima, one in the membrane

dx.doi.org/10.1021/ja310548h | J. Am. Chem. Soc. 2013, 135, 7474−7485

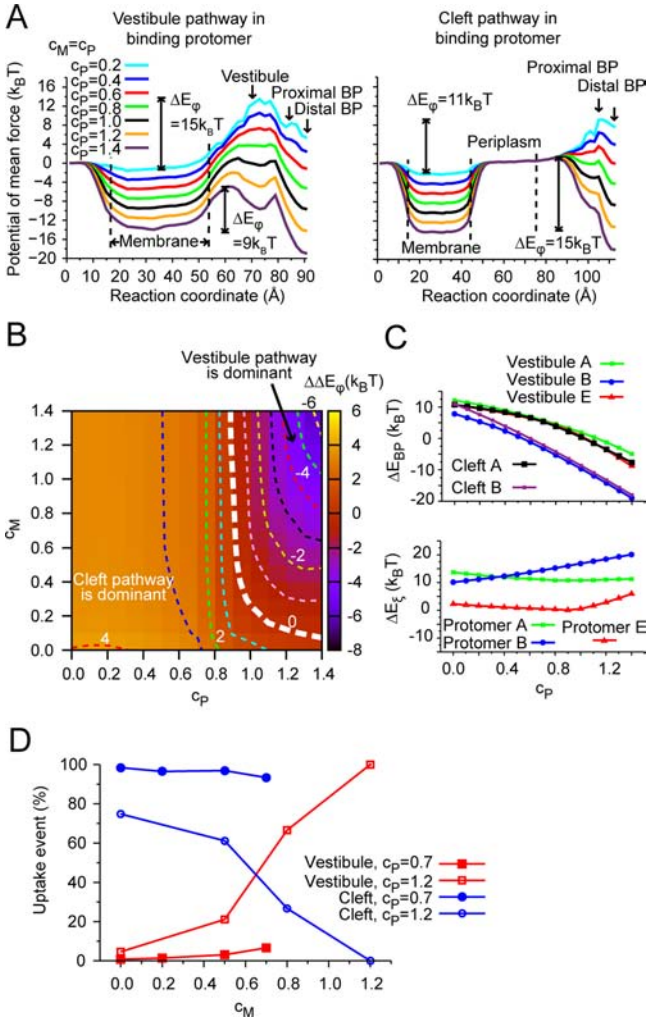

Figure 2. Ligand-dependent drug uptakes in AcrB. All results were obtained with the minocycline drug model. (A) Free energy profiles of drug uptake via the vestibule (left) and the cleft (right) paths in the B state. Multiple sets of parameters, c_P and c_M, were surveyed, and the results are illustrated by different lines. (B) The difference in the activation free energy of drug uptake, $\Delta\Delta E_\varphi = \Delta E_\varphi^{\text{vestibule}} - \Delta E_\varphi^{\text{cleft}}$, on the two-dimensional (2D) c_P and c_M space. The activation free energy, ΔE_φ^{X}, is the free energy barrier from the membrane to the proximal binding pocket (BP). The superscript indicates the pathway. Here, the comparison is made solely for protomer B. (C) Top, the binding free energy of drug in the distal BPs of the protomers A, B, and E, with the reference state in the periplasm. For protomers A and B, results calculated along different pathways are shown. Bottom, the activation energy of drug export defined by the free energy barrier from the distal BP to the exit. For both panels, $c_M = c_P$. (D) The percentage of drug uptake via a specific pathway in the dynamic simulations under various sets of parameters.

and the other at the distal binding pockets (Figure 2A). Along the vestibule pathway, the two minima are separated by a free energy barrier near the vestibule. The free energy barrier height ΔE_φ for the drug taken from the membrane depends on the two parameters, the hydrophobicity of the drug c_P and the lipophilicity of the drug c_M. As the lipophilicity increases, the free energy barrier increases, while as the hydrophobicity is strengthened, the barrier decreases (Figure S4). Along the cleft pathway, one sees a flat free energy barrier, which corresponds to the periplasm. Similar to the vestibule pathway, the free energy barrier height from the membrane increases as the lipophilicity increases.

In more details, however, the dependences of the barrier height along the two pathways on the lipophilicity and the hydrophobicity are somewhat different, which leads to the alteration of the dominant pathway depending on the property of the drug. Figure 2B plots the difference $\Delta\Delta E_\varphi$ in the free energy barriers along the two pathways, which clearly shows the boundary $\Delta\Delta E_\varphi = 0$ (the white dashed line). When both c_P and c_M are large, the vestibule pathway has a smaller barrier height and thus is dominant. Otherwise, the cleft pathway is dominant.

The alteration of the dominant uptake pathway by drugs is made possible because the vestibule and the cleft pathways have distinct locations in AcrB. Along the vestibule pathway, the proximity of the membrane surface with the entrance enables the drug not exposed to aqueous environment, which is advantageous. In contrast, the cleft is relatively far away from the membrane surface, and thus the drug is unavoidably exposed to aqueous environment during the drug uptake via the cleft. At the same time, the vestibule pathway is longer and narrower than the cleft path. Thus, clearly the balance between the two effects determines which is the dominant pathway. We note that the above analysis is in principle made for a system containing the naked AcrB: The existence of AcrA and TolC molecules may affect the conclusion substantially (see Discussion and Conclusion section).

Although the drug uptake is the main focus here, we briefly describe the drug binding and export. Again, the drug size considered here is that of minocycline. In addition, we assume $c_M = c_P$; note that the value of c_M does not affect the free energy for drug binding or export. As expected, the binding in the B state is generally much more stable than that in the states A and E regardless of the pathways, especially when c_P is large (Figure 2C top). The export in the E state is much easier than that in states A and B because the activation energy for the drug export from the distal binding pocket, ΔE_ξ, is constantly lower in the protomer E (Figure 2C bottom). Our calculations are therefore largely consistent with the functionally rotating mechanism.

Dynamic Simulations Confirm the Ligand-Dependent Uptake Mechanism. To realize direct drug uptake simulations, we introduced a simulation box, in which many minocycline molecules were put in so that the resulting drug concentration became ~34 mM. The specific high drug concentration was chosen purely for accelerating the drug uptake events. Here, assuming the functionally rotating mechanism, during the simulations we switched the energy function at certain times to realize conformational changes of the trimer from "ABE" to "BEA" and then to "EAB". Similar strategy was applied successfully for the study of the molecular motor, F_1-ATPase.[53]

Similar to the free energy analysis, we conducted simulations for diverse combinations of c_P and c_M, and for each of the parameter set, we repeated at least 100 simulation runs (in total 3800 runs; see Table 1). During the simulations, we observed a number of drug uptake and export events (in total ~3100 events), of which majority were the uptake from either vestibule or cleft pathways. Here we defined the "drug uptake" by the event that a drug molecule entered either the proximal or the distal binding pocket. On top, the simulations revealed a few additional uptake pathways (Figure S5). Some of them were very rare, such as those via the central cavity, the upper (proximal to TolC-docking domain) part of the interface between PN2 and PC1 subdomains (PN2/PC1 up) and that between PN1 and TM8. The uptakes via the exit and the lower (proximal to the

dx.doi.org/10.1021/ja310548h | J. Am. Chem. Soc. 2013, 135, 7474−7485

Table 1. Statistics of Drug Uptake Events (per 100 Trajectories)[a]

				vestibule							
c_P	c_M	vestibule access	total uptake	pathway a	pathway b	cleft	exit	central cavity	PN2/PC1 up	PN2/PC1 down	PN1/TM8
Cleft Path Dominates:											
0.00	0.00	1	1	0 (0.0)	0 (0.0)	1 (100)	0 (0.0)	0 (0.0)	0 (0.0)	0 (0.0)	0 (0.0)
0.25[b]	0.00	1.5	6	0 (0.0)	0 (0.0	6 (100)	0 (0.0)	0 (0.0)	0 (0.0)	0 (0.0)	0 (0.0)
0.40	0.00	5	21	1 (4.8)	0 (0.0)	20 (95.2)	0 (0.0)	0 (0.0)	0 (0.0)	0 (0.0)	0 (0.0)
0.40[b]	0.40	1	5	0 (0.0)	0 (0.0)	4.5 (90.0)	0.5 (10.0)	0 (0.0)	0 (0.0)	0 (0.0)	0 (0.0)
0.60	0.00	24	133	0 (0.0)	1 (0.8)	130 (97.7)	2 (1.5)	0 (0.0)	0 (0.0)	0 (0.0)	0 (0.0)
0.70	0.00	31	262	2 (0.8)	0 (0.0)	258 (98.4)	2 (0.8)	0 (0.0)	0 (0.0)	0 (0.0)	0 (0.0)
0.70	0.20	21	145	1 (0.7)	1 (0.7)	140 (96.5)	3 (2.1)	0 (0.0)	0 (0.0)	0 (0.0)	0 (0.0)
0.70	0.50	8	32	0 (0.0)	1 (3.1)	31 (96.9)	0 (0.0)	0 (0.0)	0 (0.0)	0 (0.0)	0 (0.0)
0.70[c]	0.70	0.33	5	0 (0.0)	0.33 (6.6)	4.67 (93.4)	0 (0.0)	0 (0.0)	0 (0.0)	0 (0.0)	0 (0.0)
0.80	0.00	57	396	4 (1.0)	4 (1.0)	377 (95.1)	9 (2.3)	1 (0.3)	0 (0.0)	1 (0.3)	0 (0.0)
1.00	0.00	113	766	9 (1.2)	37 (4.8)	673 (87.9)	30 (3.9)	0 (0.0)	0 (0.0)	17 (2.2)	0 (0.0)
1.00[d]	1.00	1.8	2	0.2 (10.0)	0.2 (10.0)	1.6 (80.0)	0 (0.0)	0 (0.0)	0 (0.0)	0 (0.0)	0 (0.0)
1.20	0.00	165	1030	3 (0.3)	44 (4.3)	771 (74.8)	73 (7.1)	1 (0.1)	2 (0.2)	135 (13.1)	1 (0.1)
1.20	0.50	121	232	3 (1.3)	46 (19.8)	142 (61.2)	2 (0.9)	0 (0.0)	1 (0.4)	38 (16.4)	0 (0.0)
0.76[e]	0.55	0	4.5	0 (0.0)	0 (0.0)	4.5 (100)	0 (0.0)	0 (0.0)	0 (0.0)	0 (0.0)	0 (0.0)
Vestibule Path Dominates:											
1.20	0.80	51	30	0 (0.0)	20 (66.6)	8 (26.7)	0 (0.0)	0 (0.0)	0 (0.0)	2 (6.7)	0 (0.0)
1.20[f]	1.20	3	0.91	0 (0.0)	0.91 (100)	0 (0.0)	0 (0.0)	0 (0.0)	0 (0.0)	0 (0.0)	0 (0.0)
1.40	0.80	111	63	0 (0.0)	46 (73.0)	12 (19.0)	0 (0.0)	0 (0.0)	0 (0.0)	5 (8.0)	0 (0.0)
1.40[c]	1.40	8.67	0.67	0 (0.0)	0.67 (100)	0 (0.0)	0 (0.0)	0 (0.0)	0 (0.0)	0 (0.0)	0 (0.0)
0.71[g]	0.71	560	391	11 (2.8)	204 (52.2)	96 (24.6)	32 (8.2)	1 (0.3)	0 (0.0)	44 (11.3)	3 (0.8)

[a]By default, the numbers of events in 100 simulation trajectories for minocycline were counted. Exceptions are indicated by superscripts at the left-most column. [b]Rescaled from 200 trajectories, i.e., the numbers of events in 200 trajectories were counted and divided by 2. [c]Rescaled from 300 trajectories. [d]Rescaled from 500 trajectories. [e]Rescaled from 200 trajectories for novobiocin (for convenience, c_P and c_M here were converted to mimic a virtual 6-bead model, e.g., $c_P = c_{P,8} \times 8/6$, where $c_{P,8}$ is the actual parameter used for the 8-bead novobiocin model. [f]Rescaled from 1100 trajectories for minocycline. [g]100 trajectories for acriflavine ($c_P = c_{P,3} \times 3/6$, where $c_{P,3}$ is the actual parameter used for the 3-bead acriflavine model). Number in parentheses is the percentage of all the uptake events observed in the simulations specific to each row. "Vestibule access" means the event that a drug molecule comes close to the vestibule.

transmembrane domain) part of the interface between PN2 and PC1 (PN2/PC1 down) were not so rare but were minor too. We did not investigate these minor uptake events here.

In the uptake events from near the vestibule, unexpectedly, we noticed that the route was further split into two subpathways, named the vestibule pathways a and b. Whereas the former is the pathway discovered in the structural analysis, the latter is not visible in the crystal structure. The subpathway b goes along the bottom of the porter domain in a direction toward PC1 (see Figure S5). Simulations also show that the uptake via the subpathway b is on average more frequent than that via the subpathway a (Table 1). Since the two subpathways are quite close, the vestibule pathway refers to a sum of the two subpathways a and b unless indicated otherwise.

Statistics of uptake events in the dynamic simulations is largely consistent with the results of the free energy analysis. In general, the frequency of drug uptakes is enhanced with the increase of c_P and is decreased with the increase of c_M. These dependences are somewhat different between the two uptake pathways, which results in the alteration of the dominant pathway in c_P and c_M space. (Figures S4 and S6). Thus, consistent with the free energy analysis, we found the ligand-dependent uptake mechanism. As illustrated by Figure 2D, the vestibule pathway is dominant when both c_P and c_M are large, whereas the cleft pathway is dominant otherwise. We noticed, of course, that the results are not exactly identical between the free energy analysis and the direct simulations. For example, at $c_P = 1.2$ and $c_M = 0.5$, the free energy suggests that the dominant pathway is via the vestibule (Figure 2B), yet the dynamic simulation favors the cleft.

We also investigated the effect of molecular size of the drug on the selection of uptake pathway. We performed additional two sets of simulations, including novobiocin (larger than minocycline) and acriflavine (smaller than minocycline) in the box, respectively. The hydrophobicity of novobiocin and acriflavine is very close, with the clogP values[54] 3.10 and 3.32, respectively. Minocycline is less hydrophobic, but the simulations of minocycline-shape with $c_P = 0.7$, which is in accordance to a logP value about 3.06, can be used for a comparison of size effects. For convenience, we set the c_M of each drug to be close to the corresponding c_P. The simulations showed that the smallest drug, acriflavine, took mostly the vestibule path as the dominant drug uptake pathway, with 52.2% uptake events via the vestibule path b, 2.8% the vestibule path a, and 24.6% the cleft path. Both minocycline with $c_P = 0.7$ ($c_M = 0.7$) and novobiocin favored the cleft path instead. The results imply that, in addition to the hydrophobicity and lipophilicity, the molecular size could have an effect on the uptake pathway taking by drugs.

The Stepwise Drug Uptake Dynamics. Next, based on the dynamic simulations, we address details of the drug uptake dynamics. For this purpose, we defined a 1D coordinate, P_{up}, which maps the 3D trajectory of drug movements. For each of the uptake pathways, P_{up} is defined independently characterizing the progress of drug uptake along that pathway: $P_{up} = 0$, near the geometric bottleneck (see Figure S7); $P_{up} = 1$, at the distal binding pocket. Note that the discussion here is primarily based on the simulations of minocycline, and similar conclusions could also be drawn for other drugs.

dx.doi.org/10.1021/ja310548h | J. Am. Chem. Soc. 2013, 135, 7474−7485

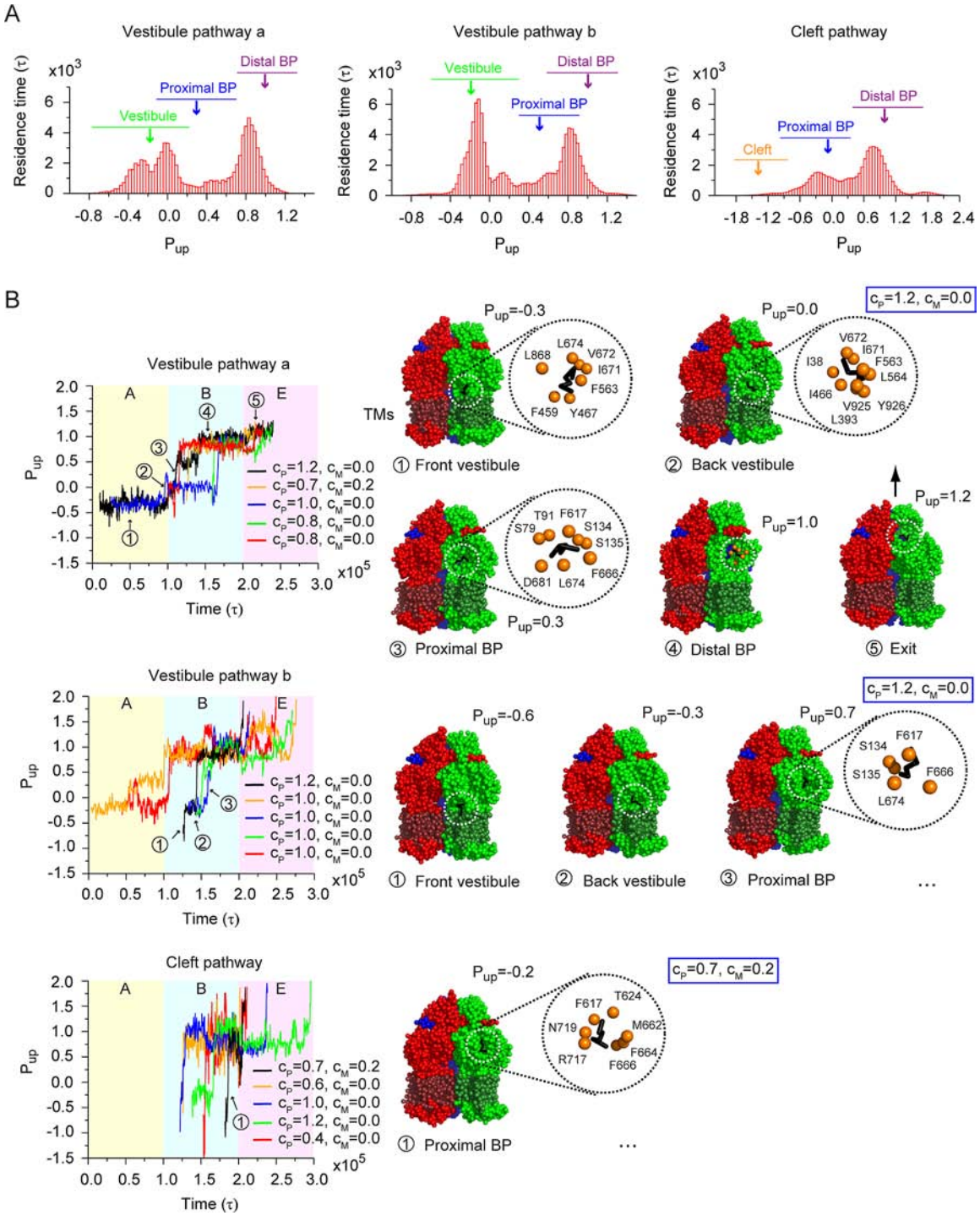

Figure 3. Trajectory analysis of drug uptake and export. The drug size considered here is that of minocycline. (A) The average drug residence time per trajectory at positions along the uptake pathways. $P_{up} = (\mathbf{r}_l - \mathbf{r}_{bot})\cdot(\mathbf{r}_{BP} - \mathbf{r}_{bot})/\|\mathbf{r}_{BP} - \mathbf{r}_{bot}\|^2$, where $\mathbf{r}_l$ is the position of the center of mass of the drug, $\mathbf{r}_{bot}$ the "bottleneck" of the path (Figure S7), and $\mathbf{r}_{BP}$ the distal binding pocket (BP). The uptake events of type A/A, A/B, and B/B were included for the counting (see text for the notation). In addition, the statistics was computed based on the partial trajectory beginning with drug uptake and ended before the conformational change to the E state or drug export. The CafeMol unit of time, τ, was used here. The result is an average over all c_P and c_M values simulated. (B) Time-series and representative snapshots of drug uptake and export. Five examples of trajectories for each uptake pathway are shown. The initial times are shifted for the comparison among drug transport in different protomers. In the snapshots, the drug is shown as black stick, and AcrB is spheres colored by chains. For clarity, atoms burying the drug are not drawn. The TMs of AcrB are indicated by shadows. The hydrophobic residues surrounding the drug during binding as well as the residues that take part in the binding of the drug in the proximal binding pocket[31] are also displayed as orange spheres.

Figure 3A shows residence time distribution of the minocycline along the 1D coordinates for the vestibule paths a (left panel) and b (middle panel) and for the cleft path (right panel), where we clearly see stepwise dynamics of drug uptakes, as proposed previously.[31−33] For vestibule subpathways a and b, clear long residence time near vestibule ($P_{up} \approx -0.2$) before

dx.doi.org/10.1021/ja310548h | J. Am. Chem. Soc. 2013, 135, 7474−7485

entering the proximal binding pocket were observed. In the proximal binding pocket (P_{up}≈0.4), the residence time is relatively short possibly because the model drug (minocycline) used here is relatively small.[31] On the other hand, for the cleft pathway, there is almost no residence near the cleft ($P_{up} \approx -1.4$), and a peak in residence time was observed in the proximal binding pocket ($P_{up} \approx -0.3$). For all cases, we see a clear peak at the distal binding pocket ($P_{up} \approx 1.0$).

It should be noted that the distribution of residence time mentioned above was averaged over the results of simulations for all the c_P and c_M values. Parameters-specific simulations may give distinct absolute values of residence time along the binding paths. For example, the simulations of minocycline uptake with specific $c_P = 0.25$ and $c_M = 0.0$ display an overall substantial reduction in residence time along the pathway (Figure S8). However, the positions of the major intermediate states of binding, which are associated with the notable peaks in the distribution before reaching the distal binding pocket, as well as the proposed stepwise binding mechanism are essentially unchanged. The argument is also supported by the independent statistics for the other two kinds of simulations, for the uptake of novobiocin and acriflavine, respectively (see Figure S8).

Next, we investigated individual drug export trajectories in structural details (Figure 3B). For the drug taken via the vestibule subpath a, the drug went through a five-step uptake and export process (Figure 3B top). At steps 1 and 2, the drug first bound to a position near the vestibule proximal to the membrane, called the "front vestibule", and then entered into a cluster of hydrophobic residues on the interface between the porter and the transmembrane domains, the "back vestibule". Notably, around the front vestibule, the residue L868 has already been shown essential for drug uptake.[37] The binding of substrates at the TM8/TM9 groove near the vestibule was also demonstrated by high-resolution crystal structures (PDB ID 2J8S[19] and 4DX5[32]). In the following steps, the drug went upward along the PC2 subdomain, entered the proximal binding pocket (step 3), and then bound to the distal binding pocket (step 4). Here the pose of the drug in the proximal binding pocket resembled the crystallographic result.[31] At step 5, the drug was exported through the exit and entered the central channel.

Similarly, the drug uptake−export via the vestibule subpath b was characterized by an initial binding to the front and back vestibules (Figure 3B middle, steps 1 and 2). The divergence of the two subpathways occurred at the back vestibule. Instead of going upward along PC2, the drug in the subpathway b went toward the PC1 subdomain, passing part of the proximal binding pocket (step 3) before entering the distal binding pocket. The subsequent process was the same as that of subpath a.

The drug dynamics in the cleft path was much simpler (Figure 3B bottom). The drug went through the cleft without encountering any long-time-staying metastable binding sites (step 1). In the proximal binding pocket, the drug shortly stayed, and the pose of drug was also similar to the results of crystallographic studies.[31,32] The export process was the same as that in the vestibule pathway. Note that in most cases drug uptake via the cleft occurred in the B protomer, which is also illustrated by the plots of representative trajectories in Figure 3B (bottom), where there is no trace in the range of A protomer.

Interplay between Conformational Switch and the Drug Uptake−Export Dynamics. Because the dynamic simulations contain a complete cycle of the functional rotation, it is interesting to investigate at which state the drug is taken into AcrB. Specifically, the A state has been suggested to bind a drug molecule as one of initial steps in the functionally rotating cycle.[17,31−33] The drug is supposed to be kicked into the distal binding pocket via peristaltic movement during the transition from the A to the B state. We classified all the drug uptake events observed in the simulations for minocycline into nine classes according to a state pattern for each pathway (Figure 4A): Each

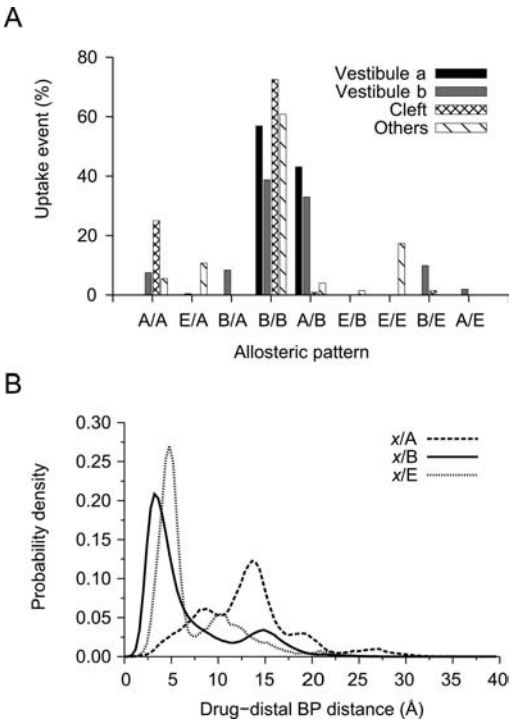

Figure 4. Coupling between drug uptake and structural switch. Results were obtained from the simulations for the minocycline. (A) The *x*-axis represents the type of conformational change during drug uptake; each pair, *u*/*v*, indicates the states before (*u*) and after (*v*) the drug entering the proximal binding pocket (BP), where *u* and *v* can be A (access), B (binding), or E (extrusion). The *y*-axis indicates the percentage of a type of drug uptake in the total uptake events along a particular pathway. The statistics was made based on the samplings of all parameter sets. (B) Distribution of the distance between drug and the distal BP. Statistics was made for the categories of drug uptake *x*/A, *x*/B, and *x*/E, respectively, where *x* means summing up all the initial states and all the possible pathways. Also, partial trajectories, when the drug has already entered the distal BP but conformational change not occurred yet, were considered.

pattern is specified by a pair of states, *x*/*y*, where *x* and *y* mean states right before the drug uptake and right after the drug reaching the proximal binding pocket (*x*, *y* = A, B, or E). Figure 4A shows that most uptake events occurred at B/B for all the pathways, indicating that the B state takes the major responsibility for the drug uptake (see also SI movies S2 and S3 for an illustration of drug uptake in B/B mode via vestibule pathway b and cleft pathway, respectively). The result is not surprising considering the drug we used for modeling is minocycline, which is small enough to go through the obstacle in the proximal binding pocket in the B state.[31]

Interestingly, significant percentages of uptake events were observed for the A/A-type pattern in the cleft pathway and A/B-type pattern in the vestibule pathway. In the A/A mode, the drug uptake essentially ended in the proximal binding pocket, since the access to the distal binding pocket in the A state is basically prohibited (Figure 4B). With a high affinity, the drug could bind

dx.doi.org/10.1021/ja310548h | J. Am. Chem. Soc. 2013, 135, 7474−7485

to the proximal binding pocket in the A state and stay there waiting for the functional rotation. On the other hand, in the A/B mode, the drug first bound to the entrance of the vestibule path in the A state and then moved to the distal binding pocket upon the A to B transition (an example in SI movie S1). The A state seems to facilitate the drug binding in the B state by a preparatory collection of the drug.

Effect of Site-Directed Mutagenesis in Putative Uptake Channel: The Vestibule Pathway b. Because the newly identified vestibule pathway b is not obvious in the crystal structures, a critical question is how far we could trust the computation and the existence of this pathway? To test it, site-directed mutagenesis experiments for AcrB in *E. coli* were thus conducted. We searched residues that are along the vestibule pathway b and that are distant from both the vestibule pathway a and the cleft pathway. To this end, we selected mutation sites Y327, T329, L137, and Q569 (shown in Figure 5 together with trajectories along the vestibule pathway b) and decided to mutate them to alanine.

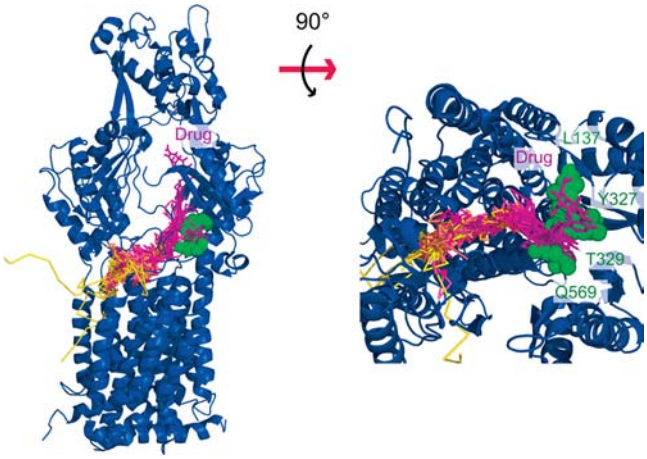

Figure 5. Comparison between simulations and site-directed mutagenesis experiments. The trace of the center of mass of the drug in the simulation (line) is superimposed onto the structure of AcrB protomer (cartoon). As examples, five trajectories of drug uptake along the vestibule path b are displayed, where the color indicates the progress of time (begin, yellow; end, magenta). The residues that were selected for site-directed mutagenesis are shown as green spheres. The drug in the distal binding pocket is also shown as sticks, and its position was taken from the crystal structure (PDB entry 2DRD).

Two single mutations Y327A and T329A, a double mutation Y327A + T329A, a triple mutation Y327A + T329A + L137A, and a quadruple mutation Y327A + T329A + L137A + Q569A were introduced into the wild-type *acrAB* gene. Plasmids containing the mutant genes as well as the wild-type gene for control (pAcBH) were transformed to the *acrAB* gene-deletion strain of *E. coli* (W3104Δ*acrAB*). The expressions of the mutants were confirmed by Western blotting (Figure S9).

All the strains were screened *in vivo* by a set of known substrates of AcrB, which includes three drugs examined in MD simulations: minocycline, acriflavine, and novobiocin. The transport activity was quantified by the minimum inhibitory concentrations (MICs) (Table 2).

First, Table 2 shows that all the tested mutations reduced resistance to most of the drugs to varying degrees, i.e., smaller MIC values than the control (the bold font). Most strikingly, the double mutations (Y327A+T329A) decreased MIC for all the compounds except ethidium bromide (ETB), and the reduction was dramatic for most of compounds. These data clearly support the finding by simulations that the vestibule pathway b contributes to the drug transport, although other possibilities cannot be ruled out.

We next compare the MIC data for the three drugs examined in MD simulations. Of the three drugs, the effect on acriflavine transport was the largest. Acriflavine efflux activity was completely abrogated to the level of *acrAB* deficient strain. As mentioned earlier, acriflavine is more hydrophobic than minocycline and is smaller than novobiocin. Thus, the result is consistent with the findings from our simulations, namely (1) the more hydrophobic drugs favor the vestibule pathway and (2) the smaller drugs favor the vestibule pathway. It should also be noted that, even for minocycline and novobiocin, the MIC data showed moderate, yet significant, decreases for the mutations targeting the vestibule pathway b. Thus, the vestibule pathway b contributes to the drug transport of all the three drugs, to some degree.

Other Supports for the Vestibule Pathway b. There are two other potential supports for the vestibule pathway b. One comes from a computational study based on molecular theory of solvation.[33] The multifunctional sites (MFS) thus detected represent the most significant binding sites for various classes of drugs. In particular, the MFS-1 predicted to be located on the lower part of the porter domain aligns the vestibule pathway b very well (Figure S10). Again, part of MFS-1 (Q569 and Q34) is specifically close to the new pathway. Second, in a recently solved high-resolution structure of AcrB,[32] we found a detergent molecule sitting near the vestibule pathway b (yellow molecule in Figure S11). This molecule is distinct from many other detergent molecules (red molecules) that are found around the TM helices and obviously mimic the lipid environment. When the TM helices are embedded into lipid membrane, the position of this yellow molecule is markedly distant from the membrane surface. We also note that many detergents are known as the substrate of AcrB.

■ DISCUSSION AND CONCLUSION

Both the free energy analysis and the dynamic simulations suggest a ligand-dependent binding mechanism in AcrB. Both the vestibule and the cleft pathways are available for drug uptake, and which one is dominant is largely dependent on the physiochemical property of the drug. With the same size of drugs, drugs that are both sufficiently hydrophobic and lipophilic favor the vestibule path, while other drugs favor the cleft pathway. In addition, with similar hydrophobicity and lipophilicity, smaller drugs tend to utilize the vestibule pathway, whereas larger drugs prefer the cleft pathway.

We should note, however, how the AcrB partners, i.e., AcrA and TolC molecules, affect the conclusion is still obscure due to the lack of the structure of AcrAB−TolC tricomplex. There has been effort in modeling the tripartite structure, but the results are somewhat controversial. For example, Symmons et al. have built a model based on *in vivo* cross-linking experiment, in which stoichiometry of AcrA and AcrB is 1 to 1, and the membrane-proximal domain of AcrA bias to the interface of protomers substantially, leaving the cleft accessible from the periplasm.[13] Nevertheless, the stoichiometry of AcrA and AcrB suggested by the surface plasmon resonance experiment[55] is 2 to 1. By this stoichiometry, with high probability the cleft pathway may be shut by the additional AcrA. The latter model also received support from the recently solved structure of CusBA complex,[56]

dx.doi.org/10.1021/ja310548h | J. Am. Chem. Soc. 2013, 135, 7474−7485

Table 2. MIC of *E. coli* W3104 Cells Lacking *acrAB* Genes Harboring Plasmids Carrying Mutant *acrAB* Gene Introduced by the Site-Directed Mutagenesis

	MIC (μg/mL)[a]											
	antibiotic							dye and others				detergent
strain and plasmid	CRM	NOV	ERY	TET	MIN	NOR	TPP	ACR	CRV	R6G	ETB	BZK
W3104	3.13 (2)	400 (1)	50 (2)	0.78 (1)	1.56 (1)	0.10 (1)	800 (4)	100 (2)	6.25 (16)	400 (4)	400 (1)	25 (16)
W3104Δ*acrAB*	0.78 (1/2)	6.25 (1/64)	1.56 (1/16)	0.20 (1/4)	0.10 (1/16)	0.025 (1/4)	6.25 (1/32)	12.5 (1/4)	<0.20 (<1/2)	1.56 (1/64)	12.5 (1/32)	1.56 (1)
pAcBH/W3104Δ*acrAB*	**1.56**	**400**	**25**	**0.78**	**1.56**	**0.10**	**200**	**50**	**0.39**	**100**	**400**	**1.56**
pAcBH(Y327A)/W3104Δ*acrAB*	0.78 (1/2)	50 (1/8)	12.5 (1/2)	0.20 (1/4)	0.39 (1/4)	0.05 (1/2)	100 (1/2)	12.5 (1/4)	0.78 (2)	6.25 (1/16)	400 (1)	<0.39 (<1/4)
pAcBH(T329A)/W3104Δ*acrAB*	3.13 (2)	100 (1/4)	1.56 (1/16)	<0.05 (<1/16)	0.78 (1/2)	0.025 (1/4)	200 (1)	6.25 (1/8)	<0.20 (<1/2)	6.25 (1/16)	400 (1)	<0.39 (<1/4)
pAcBH(Y327A,T329A)/W3104Δ*acrAB*	<0.10 (<1/16)	50 (1/8)	6.25 (1/4)	0.39 (1/2)	<0.05 (<1/32)	0.012 (1/8)	<1.56 (<1/128)	<3.13 (<1/16)	<0.20 (<1/2)	<0.78 (<1/128)	400 (1)	<0.39 (<1/4)
pAcBH(Y327A,T329A,L137A)/ W3104Δ*acrAB*	1.56 (1)	50 (1/8)	<0.20 (<1/128)	<0.05 (<1/16)	0.39 (1/4)	<0.003 (<1/32)	<1.56 (<1/128)	<3.13 (<1/16)	<0.20 (<1/2)	<0.78 (<1/128)	25 (1/16)	<0.39 (<1/4)
pAcBH(Y327A,T329A,L137A,Q569A)/ W3104Δ*acrAB*	1.56 (1)	50 (1/8)	12.5 (1/2)	0.39 (1/2)	0.78 (1/2)	0.05 (1/2)	25 (1/8)	25 (1/2)	0.39 (1)	12.5 (1/8)	200 (1/2)	1.56 (1)
clogP[b]	1.14	3.32	2.70	0.06	1.10	−1.03	5.76	3.10	5.73	5.86	5.14	5.99
c_P	0.26	0.76	0.62	0.01	0.25	NA	1.32	0.71	1.31	1.34	1.18	1.37

[a]Relative MICs were calculated as ratios between the MICs for W3104Δ*acrAB* harboring the plasmid pAcBH that carries *acrAB* gene. Abbreviations for drugs: CRM, chloramphenicol; NOV, novobiocin; ERY, erythromycin; TET, tetracycline; MIN, minocycline; NOR, norfloxacin; TPP, tetraphenylphosphonium; ACR, acriflavine; CRV, crystal violet; R6G, rhodamine 6G; ETB, ethidium bromide; BZK, benzalkonium. Values in parentheses show fold decrease/increase of MIC from that of pAcBH/W3104Δ*acrAB*. [b]clogP, the octanol/water partition coefficient calculated by XLOGP3; c_P, model parameter converted from clogP by the formula $c_P = k_BT \times \text{clogP} \times (\log 10/n_l)$, where $k_BT \approx 0.6\epsilon$, ϵ is the CafeMol unit of energy (see SI text), and $n_l = 6$ the effective number of beads in drug. NA is not available.

dx.doi.org/10.1021/ja310548h | J. Am. Chem. Soc. 2013, 135, 7474−7485

a homologous system to AcrAB. One important question to raise here is: What does our work imply if the cleft pathway is really blocked? One fact to be noted is that in Table 1 even the drugs taking the cleft path as the dominant binding pathway still have some binding events via the vestibule. It is possible that, when the cleft path is shut, all drugs will take the vestibule pathway for drug uptake. In this case, the uptake frequency of drugs previously using cleft pathway will be substantially reduced.

Previous studies mentioned a third drug uptake pathway via the central cavity of AcrB trimer.[34,57] Albeit a few observations in our simulations, the drug uptake via the central cavity is too rare to be physiologically meaningful. Recent covalent-labeling experiments did not support this path either.[37]

Moreover, we have used two parameters, c_P and c_M, to investigate the uptake of a broad range of putative drugs. The mapping of the parameters to real drugs is practically important in pharmaceutics. Approximately, logP characterizing the hydrophobicity of the drug can be converted into c_P directly (Table 2; here we uses the logP value calculated by XLOGP3).[54] By this, the c_P of typical AcrB substrates is in a range between 0.0 and 1.4, which is the range of the current survey. However, for c_M, which represents the lipophilicity of drugs, there is few experimental or theoretical data available to obtain a reasonable estimate. Although related, c_M is generally not the same as c_P, e.g., in the case of amphiphilic molecules.[51] A good estimate of c_M may come from the direct computation of the partition free energy of drugs into the water and the lipid bilayer. We emphasize that, in this study, instead of deciding on a single set of c_P and c_M values that best approximate a drug, such as minocycline, we scanned these two parameters for all the plausible range. By this, we can obtain more comprehensive insights on multidrug recognition of AcrB. Such comprehensive simulations of drug movements are practically impossible by atomistic simulation but were made possible by the use of the CG model.

Site-directed mutagenesis conducted here is not comprehensive, and there is much room left for future studies. First, not all the MIC data can be straightforwardly interpreted by the ligand-dependent drug uptake pathways proposed by the simulations. The MIC data suggested even less hydrophobic drugs may utilize the vestibule path b to some extent. On top, for complete verification of the ligand-dependent uptake pathways, we need to conduct site-directed mutations specific to the cleft pathway and those specific to the vestibule pathway a.

Finally the model here assumes the main driving force for drug uptake is the hydrophobic interaction. Undoubtedly, other types of forces, such as hydrophilic and ionic interactions, could have effects on protein-drug binding, too, especially in stabilizing the drug in a specific binding pose.[17,31,32] The simplification of interactions implies that the computational results reported here should be understood in a more qualitative way, and one should be cautious to compare the exact values of quantities presented in this work, such as the relative free energy, the residence time distribution, and the binding rate, to their physical correspondence. Furthermore, the model neglected some of the physiochemical properties of drugs, such as the ordering of amphiphilic drugs in the lipid bilayer and the conformational flexibility of drugs with rotatable bonds. The effects of such properties on drug uptake need to be further evaluated.

EXPERIMENTAL SECTION

We briefly summarize the models and simulation protocols here, and the complete description of the method is found in the SI text. The experiments are fully described here.

Modeling Protein and Drug. The protein was simplified by using two beads per one amino acid (one bead for glycine), placed on the position of C_α atom and the center of mass of the side chain, respectively. The AICG model[49] was employed for the interactions in proteins, with the use of the asymmetric crystal structure of AcrB (PDB ID 2J8S)[19] adopted as the reference. The drug was described as a rigid linear chain with six, three, and eight CG beads for minocycline, acriflavine, and novobiocin, respectively. The crystal structures with PDB ID 2DRD[17] and 1S14[58] were adopted as reference structures for minocycline and novobiocin, respectively. The reference structure for acriflavine was obtained from ZINC database.[59]

In the protein model, the bead representing the side chain has bonded interacting terms with local C_α and side chain beads but has no interaction with nonlocal protein beads; however, both C_α and side chain beads have an excluded volume effect on the drug. The hydrophobic interaction between the drug and the side chain of hydrophobic residues, defined by Phe, Ile, Leu, Val, Trp, and Tyr, was considered in the same functional form as in previous work:[30]

$$V_{HP} = -c_P \varepsilon \sum_{\substack{i \text{ in drug or} \\ \text{hydrophobic} \\ \text{residues}}} S_{HP}(\rho_i) \tag{1}$$

where c_P scales the strength of the interaction, $S_{HP}(\rho_i)$ the "buriedness" of bead i with local density ρ_i, and ε the unit of energy. In eq 1, the TMs, defined by the Orientations of Proteins in Membranes database,[60] were precluded from the calculation. Note that except for the definition of TMs, there is no particular region that specifically defined in the simulations. Therefore, how the drug and protein are associated is largely prediction of our model.

A simple rounded square well potential was exploited to account for the association of drugs as well as TMs with the membrane:

$$V_{mem} = \begin{cases} 0 & |z| \geq \delta_{max} \\ -c_M \varepsilon & |z| \leq \delta_{min} \\ -\frac{1}{2} c_M \varepsilon \left[1 + \cos\left(\pi \frac{z - \delta_{min}}{\delta_{max} - \delta_{min}} \right) \right] & \delta_{min} < z < \delta_{max} \\ -\frac{1}{2} c_M \varepsilon \left[1 - \cos\left(\pi \frac{z + \delta_{max}}{\delta_{max} - \delta_{min}} \right) \right] & -\delta_{max} < z < -\delta_{min} \end{cases} \tag{2}$$

where z is the coordinate of the bead along the direction normal to the membrane and c_M the well depth. For TMs, c_M is a constant equal to 3.6. $\delta_{max} = d_{mem} + 0.5$ Å, $\delta_{min} = d_{mem} - 0.5$ Å, and $d_{mem} = 30$ Å the thickness of the membrane.

Free Energy Calculation. The umbrella sampling and the weighted histogram analysis method[61] were employed for the calculation of the free energy profiles of drug uptake and export. For the vestibule and exit tunnels, the reaction coordinates (RCs) indicate the movement of drug along single lines approximately parallel to the tunnels. For the cleft pathway, the RC is divided into two parts. First, starting from a position below AcrB, the drug is moved to the periplasm along the direction normal to the membrane surface. Second, in parallel to the membrane surface, the drug is moved into the distal binding pocket of AcrB via the cleft gate (Figure S1). In A and B protomers, the free energy profiles of all the pathways were measured, while in E protomer only the exit path. All the free energies were made comparable by the facts that (1) the free energy of the cytoplasmic ends of all pathways was zero, (2) the free energy difference between the distal binding pocket of the vestibule and the exit pathways was estimated by the thermodynamic integration, and (3) similar calculation was also made to estimate the free energy

dx.doi.org/10.1021/ja310548h | J. Am. Chem. Soc. 2013, 135, 7474−7485

difference between the exit ends of the exit pathways in B and E protomers.

All initial conformations of the sampling were generated by a constant-velocity steered MD simulation along the RC, with structures saved at an interval of 1 Å. In addition to the harmonic potential with respect to RC, we applied extra radial distance constraint on the drug with respect to the RC to prevent it from diffusing away from the pathway. One set of parameters, $c_P = 1.0$ and $c_M = 1.0$, was adopted for the sampling, and the results for other parameter sets were obtained by reweighting.[52] All the simulations were carried out in Langevin dynamics with temperature T = 300 K. For sampling, 1.0×10^5 steps of equilibration followed by 2.0×10^6 steps of production were performed, with the step size of integration equal to 0.1τ, where τ is the unit of time (see SI text). The coordinates were saved every 1000 steps, accumulating a total of 2000 samples for each constrained position.

Dynamic Simulation. The dynamics of drug uptake in AcrB was investigated by a large set of dynamic simulations surveying a broad range of values (0.0−1.4) for parameters c_P and c_M. For each set of parameters, at least 100 trajectories were sampled with each guided by Langevin dynamics at the temperature T = 300 K and carried out in a $230 \times 230 \times 250$ (Å^3) box. The TMs were initially inserted into the implicit membrane. The drug molecules were initially placed arbitarily in the box but quickly reached an equilibrium partition into membrane based on the c_M values. The conformational change of AcrB was realized by switching the reference states of the AICG potential obeying the order defined by the functionally rotating mechanism: Starting with ABE state, we first switched the reference state to BEA and then switched to EAB. For each state, 1.0×10^6 steps of time integration were performed with a step size of 0.1τ and structures saved every 1000 steps.

All the calculations mentioned above were performed by the CafeMol package[62] with slight modification of the source codes.

Bacterial Strains and Plasmids. *E. coli* strains JM109[63] and W3104[64] were used for DNA manipulation, DNA sequencing, site-directed mutagenesis, and investigation of phenotypes of the mutants, respectively. Strain W3104Δ*acrAB*[65] is the *acrAB* gene-deletion derivatives of *E. coli* W3104. Plasmids pAcBH, a derivative of pUC118 which clones *acrR*, *acrA*, and His-tagged *acrB* gene were prepared previously.[66]

Site-Directed Mutagenesis. Point mutations were introduced by the use of QuikChange site-directed mutagenesis kit (Stratagene) with mutagenic primers to create the following codon replacements: Y327A T329A (TACRGCG ACCRGCG), Y327A (TACRGCG), T329A (ACCRGCG), L137A (CTGRGCG), and Q569A (CAGRGCG). The constructed plasmids were sequenced using a 3730xl DNA Analyzer (Applied Biosystems, U.S.A.) to ensure the presence of the desired mutation. The resulting mutant AcrB proteins have a polyhistidine tag on the carboxy terminus similarly to wild-type AcrB.

Drug Resistance Determination. The MICs of drugs and toxic compounds were determined as the concentrations that greatly prevented bacterial growth on YT-agar (0.8% tryptone, 0.5% yeast extract, and 0.5% NaCl) plates with sequential 2-fold dilutions, as described previously.[67]

Expression of AcrB and AcrB Mutants. *E. coli* W3104Δ*acrAB* was used for expression of the AcrB and AcrB mutants. All proteins have a six-histidine tag at the carboxyl terminal. Membrane fraction was prepared by ultracentrifugation as described previously[68] and subjected to Western blotting with a mouse antipoly histidine antibody (Sigma).

■ ASSOCIATED CONTENT

Ⓢ Supporting Information

Details of the method, Figures S1−S11, movies S1−S3 are included in the supporting materials. This information is available free of charge via the Internet at http://pubs.acs.org.

■ AUTHOR INFORMATION

Corresponding Author

takada@biophys.kyoto-u.ac.jp

Notes

The authors declare no competing financial interest.

■ ACKNOWLEDGMENTS

We thank Tsutomu Yamane, Takashi Imai, Akinori Kidera, and Mitsunori Ikeguchi for beneficial discussions. This work was supported partly by Research and Development of the Next-Generation Integrated Simulation of Living Matter, partly by Grant-in-Aid for Scientific Researches from the Ministry of Education, Culture, Sports, Science, and Technology of Japan, partly by the "Funding Program for World-Leading Innovative R&D on Science and Technology" of the Japan Society for the Promotion of Science initiated by the Council for Science and Technology Policy, and partly by Exploratory Research for Advanced Technology Murata Lipid Active Structure Project of the Japan Science and Technology Agency.

■ REFERENCES

(1) Nikaido, H.; Takatsuka, Y. *Biochim. Biophys. Acta* **2009**, *1794*, 769.
(2) Li, X. Z.; Nikaido, H. *Drugs* **2004**, *64*, 159.
(3) Higgins, C. F. *Nature* **2007**, *446*, 749.
(4) Ma, D.; Cook, D. N.; Alberti, M.; Pon, N. G.; Nikaido, H.; Hearst, J. E. *J. Bacteriol.* **1993**, *175*, 6299.
(5) Ma, D.; Cook, D. N.; Alberti, M.; Pon, N. G.; Nikaido, H.; Hearst, J. E. *Mol. Microbiol.* **1995**, *16*, 45.
(6) Okusu, H.; Ma, D.; Nikaido, H. *J. Bacteriol.* **1996**, *178*, 306.
(7) Fralick, J. A. *J. Bacteriol.* **1996**, *178*, 5803.
(8) Sulavik, M. C.; Houseweart, C.; Cramer, C.; Jiwani, N.; Murgolo, N.; Greene, J.; DiDomenico, B.; Shaw, K. J.; Miller, G. H.; Hare, R.; Shimer, G. *Antimicrob. Agents Chemother.* **2001**, *45*, 1126.
(9) Zgurskaya, H. I.; Nikaido, H. *J. Bacteriol.* **2000**, *182*, 4264.
(10) Tikhonova, E. B.; Zgurskaya, H. I. *J. Biol. Chem.* **2004**, *279*, 32116.
(11) Tamura, N.; Murakami, S.; Oyama, Y.; Ishiguro, M.; Yamaguchi, A. *Biochemistry* **2005**, *44*, 11115.
(12) Lobedanz, S.; Bokma, E.; Symmons, M. F.; Koronakis, E.; Hughes, C.; Koronakis, V. *Proc. Natl. Acad. Sci. U.S.A.* **2007**, *104*, 4612.
(13) Symmons, M. F.; Bokma, E.; Koronakis, E.; Hughes, C.; Koronakis, V. *Proc. Natl. Acad. Sci. U.S.A.* **2009**, *106*, 7173.
(14) Zgurskaya, H. I.; Nikaido, H. *Proc. Natl. Acad. Sci. U.S.A.* **1999**, *96*, 7190.
(15) Murakami, S. *Curr. Opin. Struct. Biol.* **2008**, *18*, 459.
(16) Murakami, S.; Nakashima, R.; Yamashita, E.; Yamaguchi, A. *Nature* **2002**, *419*, 587.
(17) Murakami, S.; Nakashima, R.; Yamashita, E.; Matsumoto, T.; Yamaguchi, A. *Nature* **2006**, *443*, 173.
(18) Seeger, M. A.; Schiefner, A.; Eicher, T.; Verrey, F.; Diederichs, K.; Pos, K. M. *Science* **2006**, *313*, 1295.
(19) Sennhauser, G.; Amstutz, P.; Briand, C.; Storchenegger, O.; Grutter, M. G. *PLoS Biol.* **2007**, *5*, e7.
(20) Bohnert, J. A.; Schuster, S.; Seeger, M. A.; Fahnrich, E.; Pos, K. M.; Kern, W. V. *J. Bacteriol.* **2008**, *190*, 8225.
(21) Takatsuka, Y.; Chen, C.; Nikaido, H. *Proc. Natl. Acad. Sci. U.S.A.* **2010**, *107*, 6559.
(22) Smart, O. S.; Neduvelil, J. G.; Wang, X.; Wallace, B. A.; Sansom, M. S. *J. Mol. Graphics* **1996**, *14*, 354.
(23) Humphrey, W.; Dalke, A.; Schulten, K. *J. Mol. Graphics* **1996**, *14*, 33.
(24) *PyMol*; Schrodinger, LLC: New York, 2010.
(25) Jardetzky, O. *Nature* **1966**, *211*, 969.
(26) Takatsuka, Y.; Nikaido, H. *J. Bacteriol.* **2007**, *189*, 8677.
(27) Seeger, M. A.; von Ballmoos, C.; Eicher, T.; Brandstatter, L.; Verrey, F.; Diederichs, K.; Pos, K. M. *Nat. Struct. Mol. Biol.* **2008**, *15*, 199.
(28) Takatsuka, Y.; Nikaido, H. *J. Bacteriol.* **2009**, *191*, 1729.
(29) Schulz, R.; Vargiu, A. V.; Collu, F.; Kleinekathofer, U.; Ruggerone, P. *PLoS Comput. Biol.* **2010**, *6*, e1000806.

(30) Yao, X. Q.; Kenzaki, H.; Murakami, S.; Takada, S. *Nat. Commun.* **2010**, *1*, 117.
(31) Nakashima, R.; Sakurai, K.; Yamasaki, S.; Nishino, K.; Yamaguchi, A. *Nature* **2011**, *480*, 565.
(32) Eicher, T.; Cha, H. J.; Seeger, M. A.; Brandstatter, L.; El-Delik, J.; Bohnert, J. A.; Kern, W. V.; Verrey, F.; Grutter, M. G.; Diederichs, K.; Pos, K. M. *Proc. Natl. Acad. Sci. U.S.A.* **2012**, *109*, 5687.
(33) Imai, T.; Miyashita, N.; Sugita, Y.; Kovalenko, A.; Hirata, F.; Kidera, A. *J. Phys. Chem. B* **2011**, *115*, 8288.
(34) Yu, E. W.; Aires, J. R.; McDermott, G.; Nikaido, H. *J. Bacteriol.* **2005**, *187*, 6804.
(35) Drew, D.; Klepsch, M. M.; Newstead, S.; Flaig, R.; De Gier, J. W.; Iwata, S.; Beis, K. *Mol. Membr. Biol.* **2008**, *25*, 677.
(36) Husain, F.; Nikaido, H. *Mol. Microbiol.* **2010**, *78*, 320.
(37) Husain, F.; Bikhchandani, M.; Nikaido, H. *J. Bacteriol.* **2011**, *19*, 19.
(38) Fischer, N.; Kandt, C. *Proteins* **2011**, *79*, 2871.
(39) Wang, B.; Weng, J.; Fan, K.; Wang, W. *Proteins: Struct., Funct., Bioinf.* **2011**, *79*, 2936.
(40) Schulz, R.; Vargiu, A. V.; Ruggerone, P.; Kleinekathofer, U. *J. Phys. Chem. B* **2011**, *115*, 8278.
(41) Vargiu, A. V.; Collu, F.; Schulz, R.; Pos, K. M.; Zacharias, M.; Kleinekathofer, U.; Ruggerone, P. *J. Am. Chem. Soc.* **2011**, *133*, 10704.
(42) Raunest, M.; Kandt, C. *Biochemistry* **2012**, *51*, 1719.
(43) Wang, B.; Weng, J.; Fan, K.; Wang, W. *J. Phys. Chem. B* **2012**, *116*, 3411.
(44) Vargiu, A. V.; Nikaido, H. *Proc. Natl. Acad. Sci. U.S.A.* **2012**, *109*, 20637.
(45) Feng, Z.; Hou, T.; Li, Y. *Mol. Biosyst.* **2012**, *8*, 2699.
(46) Fischer, N.; Kandt, C. *Biochim. Biophys. Acta* **2013**, *1828*, 632.
(47) Pos, K. M. *Biochim. Biophys. Acta* **2009**, *1794*, 782.
(48) Onuchic, J. N.; Luthey-Schulten, Z.; Wolynes, P. G. *Annu. Rev. Phys. Chem.* **1997**, *48*, 545.
(49) Li, W.; Wolynes, P. G.; Takada, S. *Proc. Natl. Acad. Sci. U.S.A.* **2011**, *108*, 3504.
(50) Li, W.; Yoshii, H.; Hori, N.; Kameda, T.; Takada, S. *Methods* **2010**, *52*, 106.
(51) Giaginis, C.; Tsantili-Kakoulidou, A. *J. Pharm. Sci.* **2008**, *97*, 2984.
(52) Ferrenberg, A. M.; Swendsen, R. H. *Phys. Rev. Lett.* **1989**, *63*, 1195.
(53) Koga, N.; Takada, S. *Proc. Natl. Acad. Sci. U.S.A.* **2006**, *103*, 5367.
(54) Cheng, T.; Zhao, Y.; Li, X.; Lin, F.; Xu, Y.; Zhang, X.; Li, Y.; Wang, R.; Lai, L. *J. Chem. Inf. Model.* **2007**, *47*, 2140.
(55) Tikhonova, E. B.; Yamada, Y.; Zgurskaya, H. I. *Chem. Biol.* **2011**, *18*, 454.
(56) Su, C. C.; Long, F.; Zimmermann, M. T.; Rajashankar, K. R.; Jernigan, R. L.; Yu, E. W. *Nature* **2011**, *470*, 558.
(57) Yu, E. W.; McDermott, G.; Zgurskaya, H. I.; Nikaido, H.; Koshland, D. E., Jr. *Science* **2003**, *300*, 976.
(58) Bellon, S.; Parsons, J. D.; Wei, Y.; Hayakawa, K.; Swenson, L. L.; Charifson, P. S.; Lippke, J. A.; Aldape, R.; Gross, C. H. *Antimicrob. Agents Chemother.* **2004**, *48*, 1856.
(59) Irwin, J. J.; Sterling, T.; Mysinger, M. M.; Bolstad, E. S.; Coleman, R. G. *J. Chem. Inf. Model.* **2012**, *52*, 1757.
(60) Lomize, M. A.; Lomize, A. L.; Pogozheva, I. D.; Mosberg, H. I. *Bioinformatics* **2006**, *22*, 623.
(61) Kumar, S.; Bouzida, D.; Swendsen, R. H.; Kollman, P. A.; Rosenberg, J. M. *J. Comput. Chem.* **1992**, *13*, 1011.
(62) Kenzaki, H.; Koga, N.; Hori, N.; Kanada, R.; Li, W.; Okazaki, K.-i.; Yao, X.-Q.; Takada, S. *J. Chem. Theory Comput.* **2011**, *7*, 1979.
(63) Yanisch-Perron, C.; Vieira, J.; Messing, J. *Gene* **1985**, *33*, 103.
(64) Yamamoto, T.; Tanaka, M.; Nohara, C.; Fukunaga, Y.; Yamagishi, S. *J. Bacteriol.* **1981**, *145*, 808.
(65) Kobayashi, N.; Nishino, K.; Hirata, T.; Yamaguchi, A. *FEBS Lett.* **2003**, *546*, 241.
(66) Fujihira, E.; Tamura, N.; Yamaguchi, A. *J. Biochem.* **2002**, *131*, 145.
(67) Nishino, K.; Yamaguchi, A. *J. Bacteriol.* **2001**, *183*, 5803.
(68) Murakami, S.; Tamura, N.; Saito, A.; Hirata, T.; Yamaguchi, A. *J. Biol. Chem.* **2004**, *279*, 3743.